Post Challenge Effects of Ozg-38.61.3 Gamma Irradiated SARS-CoV-2 Vaccine on Organ Protection in Transgenic Mouse Model

Mustafa Öztatlıcı¹, Derya Dilek Kançağı^{2,3}, Hülya Öztatlıcı⁴, Raife Dilek Turan^{3,5}, Gözde Sır Karakuş³, Bulut Yurtsever^{3,6}, Didem Çakırsoy^{3,7}, Selen Abanuz^{3,6}, Cihan Taştan^{3,8}, Samed Özer⁹, Gamze Tümentemur¹⁰, Murat Kasap¹¹, Gürler Akpınar¹¹, Büşra Şen Halıcıoğlu⁴, Sevda Demir⁵, Dilek Telci⁵, Fikrettin Şahin⁵, Mehmet İbrahim Tuğlu¹², Ercüment Ovali³

- ¹Department of Histology and Embryology, Gaziantep Islam Science and Technology University, Gaziantep, Türkiye.
- ² Biochemistry Department, Faculty of Pharmacy, Fenerbahçe University, İstanbul, Türkiye.
- ³ Acibadem Labcell Cellular Therapy Laboratory, Istanbul, Türkiye.
- ⁴ Department of Histology and Embryology, Gaziantep University, Gaziantep, Türkiye.
- ⁵ Genetic and Bioengineering Department, Yeditepe University, Istanbul, Türkiye.
- ⁶ Medical Biochemistry Department, Acıbadem Mehmet Ali Aydınlar University, İstanbul, Türkiye.
- ⁷ Medical Biotechnology Department, Acıbadem Mehmet Ali Aydınlar University, İstanbul, Türkiye.
- ⁸ Molecular Biology and Genetics Department, Üsküdar University, İstanbul, Türkiye.
- ⁹ Animal Application and Research Center, Acıbadem Mehmet Ali Aydınlar University, İstanbul, Türkiye.
- ¹⁰ Vocational School of Health Services, Acıbadem Mehmet Ali Aydınlar University, İstanbul, Türkiye.
- ¹¹ Department of Medical Biology, Medical School of Kocaeli University, Kocaeli, Türkiye.
- ¹² Department of Histology and Embryology, Manisa Celal Bayar University, Manisa, Türkiye

Correspondence Author: Derya Dilek Kancağı

E-mail: derya.kancagi@gmail.com

Received: July 10,2024 Accepted: September 5, 2025

ABSTRACT

Objective: Coronavirus disease 2019 (COVID-19) is an infectious outbreak caused by the severe acute respiratory syndrome coronavirus 2 (SARS-CoV-2) and virus-related deaths are increasing day by day. For this reason, vaccine studies and their urgent use are of great importance to prevent the pandemic. In this study, multi-organ damages caused by SARS-CoV-2 virus in human – angiotensin-converting enzyme type 2 (ACE2) transgenic mice and the protective effects of OZG-38.61.3 gamma irradiated SARS-CoV-2 vaccine against viral damage were investigated.

Methods: For this purpose, transgenic K18-hACE2 BALB/c mice were randomly allocated into 4 groups, negative control group (NC), positive control group (PC, SARS-CoV-2 infected), and 2 different doses of OZG-38.61.3 vaccine (Challenge 1, dose of 10¹³ and Ch2, 10¹⁴ viral particle after SARS-CoV-2 infection). After the administrations, lung, heart and kidney tissues were examined by histopathological, immunohistochemical and TUNEL analysis.

Results: Our results showed that the vaccine doses decreased the apoptosis, oxidative stress and inflammation parameters caused by virus in lung, heart, and kidney tissues. It was also found that the vaccine protected the expressions of tight junction proteins in the kidneys.

Conclusion: According to our findings, it is suggested that the OZG-38.61.3 can be an effective and protective vaccine that can be safely used against the SARS-CoV-2 virus.

Keywords: COVID-19, SARS-CoV-2, human ACE2 transgenic mouse, Organ damage, Vaccination

1. INTRODUCTION

Coronavirus disease 2019 (COVID-19), caused by severe acute respiratory syndrome 2 RNA virus, called the new type of Coronavirus (SARS-CoV-2), is an infectious disease (1). After the COVID-19 disease was first seen in Wuhan, China, it spread rapidly around the world and was declared a global pandemic by WHO on March 11, 2020.

Taxonomically, SARS-CoV-2 is classified as a member of the SARS-related coronavirus (SARS-CoV) in the betacoronavirus

(βCoV) genus of the Coronaviridae family (2). There are three transmembrane proteins in the lipid bilayer: Spike (S) protein, envelope (E) protein and membrane (M) protein (3). Spike proteins present on the virus bind to angiotensin converting enzyme 2 (ACE2) receptors to enter the host cell, and the viral envelope fuses with the cellular membranes. Thus, the viral genome enters the host cell (4). Expression of the ACE2 receptor on the surface of alveolar epithelial type II cells, heart, kidney, intestine and endothelial cells make these cells

How to cite this article: Öztatlıcı M, Kançağı D.D, Öztatlıcı H, Turan D.R, Karakuş Sır G, Yurtsever B, Çakırsoy D, Abanuz S, Taştan C, Özer S, Tümentemur G, Kasap M, Akpınar G, Halıcıoğlu Şen B, Demir S, Telci D, Şahin F, Tuğlu İ.B, Ovalı E. Post Challenge Effects Of Ozg-38.61.3 Gamma Irradiated SARS-CoV-2 Vaccine On Organ Protection In Transgenic Mouse Model. Clin Exp Health Sci 2025; 15: 504-516. https://doi.org/10.33808/clinexphealthsci.1512385

Copyright © 2025 Marmara University Press



and organs as a target for SARS-CoV-2 (1). The immune system perceives the emitted viral particles as foreign and presents them to natural killer and cytotoxic T cells. Thus, the immune system is activated by the production of high amounts of proinflammatory cytokines and chemokines. As a result of the activation of the immune system more than normal, cytokine storm develops, and multi-organ failure is seen with thrombotic tendency.

Appropriate animal models are needed to elucidate the pathogenesis of the disease and to develop effective vaccines or therapeutics (5). As stated in our previous study, mice are generally preferred in antiviral studies due to their protein similarities and simple genetic structures (6). However, while SARS-CoV-2 can use human, bat, and civet angiotensin-converting enzyme type 2 (ACE2) receptors for entry into target cells, classical experimental mice do not have these receptors. Therefore, human ACE2 (hACE2) receptor-encoding transgenic mice were preferred in this study. In our previous study, the protection and safety of the OZG-38.61.3 vaccine candidate against SARS-CoV-2 infection was demonstrated.

In this study, the effects of OZG-38.61.3 vaccine, which is a candidate for COVID-19 treatment, on intense inflammation and oxidative stress in SARS-CoV-2 infection, as mentioned above, were evaluated. In this study, it was tested how protective OZG-38.61.3 could be in controlling the damage caused by the virus after viral challenge.

2. METHODS

2.1. SARS-CoV-2 isolation-propagation and cell culture

Nasopharyngeal and oropharyngeal cavity samples were obtained from patients who were diagnosed as COVID-19 by Real-Time PCR in Acıbadem Altunizade Hospital, Acıbadem Mehmet Ali Aydınlar University Atakent, and Maslak Hospitals. The study design was approved by the Ethics Committee of Acıbadem Mehmet Ali Aydınlar University (ATADEK-2020/05/41). All techniques had been executed according to the applicable guidelines. The SARS-CoV-2 isolation-propagation and cell culture was reported in our previous report (7)

2.2. Inactivation of SARS-CoV-2

2.2.1. Gamma irradiation and Glutaraldehyde mediated inactivation kinetics

In order to perform the gamma irradiation mediated inactivation kinetics study, 5 different dose ranges between 3-65 kGy were decided (3-7 kGy, 10-25 kGy, 18-35 kGy, 25-45 kGy, 45-65 kGy). After gamma irradiation inactivation at different doses were completed, colorimetric MTT assay was performed to evaluate the viability of Vero cells cocultured with vaccine for 72 hours. For glutaraldehyde inactivation, viruses were inactivated and fixed with 2.5% glutaraldehyde in PBS (0.1 M, pH 7.2) for 2.5 h.

2.2.2. Quantitative RT-PCR to determine viral RNA copy number

Total RNA isolations were performed from gamma and glutaraldehyde inactivated samples using Direct-zol RNA Miniprep

Kits (Zymo Research, USA), and concentrations were determined using QUBIT fluorometer with the QUBIT RNA HS Assay (Thermo Fisher Scientific, USA). Quantitative RT-PCR was performed with the QuantiVirus SARS-CoV-2 Test Kit (Diacarta) according to the manufacturer's protocol. The quantitative RT-PCR analysis was analyzed in Roche Lightcycler 96.

2.2.3. Single immunodiffusion assay

This method was modified from single radial immunodiffusion assay (8). The protocol was described in our previous report (6).

2.2.4. Two-dimensional (2D) gel electrophoresis

SARS-CoV-2 (active virus), gamma and glutaraldehyde inactivated samples were concentrated with 3K ultrafiltration spin filters (Amicon Ultra Centrifugal Filters 3K Cat no UFC500396, Millipore) in the BSL-3 laboratory, and focusing buffer containing chaotropic agent (8 M urea, 2% (w/v) CHAPS, 50 mM DTT, % 0.2 3-10 ampholyte, 0.001% bromphenol blue) was added in equal volume (50µL) upon our recommendation. The added buffer inactivated all virus particles in the samples and made the protein content workable. 20 µg of each sample was subjected to 2D gel electrophoresis based on the Bradford measurement method. Prepared samples were soaked in 7 cm pH 3-10 NL IPG strips by passive rehydration method overnight. After rehydration, the proteins were focused at an increased voltage of 25,000V in total. After focusing, the strips were washed with Buffer I (6 M Urea, 0.375 M Tris. HCl pH 8.8, 2% SDS, 20% Glycerol, 2% (w/v) DTT) and II (6 M Urea, 0.375 M Tris.HCl pH 8.8, % 2 SDS, 20% Glycerol, 2.5% (w/v) Iodine Acetamide) for 15 minutes and separated in 12% keratin-free SDS-PAGE gels at 180V current. When the run were completed the gels were fixed and then the protein spots were made visible by silver staining, a sensitive protein staining technique.

2.2.5. Cytokine Bead Array (CBA) as an Immunogenicity Assay

Following the isolation of peripheral mononuclear cells (PBMC) by overlaying blood on FicollPaque Plus (GE Healthcare Bio-Sciences AB, Uppsala, Sweden), 18-35 kGy, 25-45 kGy, 45-65 kGy gamma irradiated vaccine samples were incubated with PBMCs at 37°C for 24 hours. To analyze IFNy level, MACSPLEX Cytokine 12 kit, human (Miltenyi Biotec) was used for the Cytokine bead array following the manufacturer's protocol. And then samples were collected into sample tubes, and flow analysis was done. Flow analysis was performed with the MACSQUANT Analyzer (Miltenyi Biotec).

2.3. Challenge Assay

2.3.1. OZG-38.61.3 inactivated SARS-CoV-2 vaccine production and Transgenic animal study

During virus replication, 90% confluent Vero cells in cell culture flasks with a larger surface area were gradually cultured with virus-containing supernatant. The virus was

concentrated by centrifugation in a special tube with a 100 KDa filter. The concentrated virus was stored at – 80 °C before irradiation. All concentrated viruses obtained are pooled and washed two times with distilled water for diafiltration in a 100 KDa concentrator. The concentrated virus mixture was decided to be inactivated by irradiation at 25 kGy because of kinetic study performed. Transgenic animal study was carried out with respect to the protocol reported in our previous study (6). Transgenic animal study was made by using nonlethal TCID50 dose to observe the protection and especially the effect of antibody dependent enhancement in viral challenge. TCID50 dose of SARS-CoV-2 were calculated and published in our previous study (6,9).

2.3.2. Histopathological Examination, Immunohistochemistry and TUNEL Assay

Lung, heart and kidney tissues were taken immediately after dissection and fixed in 10% and embedded in paraffin. Sections (5 μ mthick) were stained with H&E and Masson's trichrome. Ashcroft scoring method was used for histopathological evaluations of pulmonary fibrosis. Immunohistochemical analyses were performed as described previously. The monoclonal antibodies used were Caspase-3, iNOS, IL-6, IL-10, TGF- β 1, eNOS, TNF- α , Occludin and Claudin-1 (10,11).

To examine in situ cell apoptosis, the 5-µm thick sections of the lung, heart and kidney tissues were used for TUNEL staining. The TUNEL method was performed according to the manufacturer's (Millipore, 2869035) instructions (12).

2.4. Statistical Analysis

Normally distributed data in bar graphs was tested using student's t-tests for two independent means. The Mann–Whitney U test was employed for comparison between two groups of non-normally distributed data. Each data point represents an independent measurement. Bar plots report the mean and standard deviation of the mean.

3. RESULTS

3.1. The Effectiveness of Gamma Irradiation Inactivation Results

3.1.1. Gamma Irradiation Inactivation Kinetics

As a result of the analyzes made with the product obtained by 5 different dose range between 3-65 kGy of gamma irradiation, it was found that the safe inactivation range for SARS-CoV-2 started above >25 kGy (Supplementary Figure 1A), but when it exceeded 45 kGy, it has been observed that viruses cause a significant decrease in antigenic expression ability, T cell stimulation ability and viral RNA copy number (7). Therefore, it has been confirmed that the ideal dose range is 25 kGy in terms of inactivity and immunogenicity.

Changes in viral RNA copy number were compared between non-inactivated, gamma-inactivated and chemically inactivated viruses, and gamma irradiation inactivation was shown to preserve RNA copy number more effectively than chemical inactivation. It was determined that 7 times higher viral RNA copy number could be preserved with gamma irradiation (Supplementary Figure 1B).

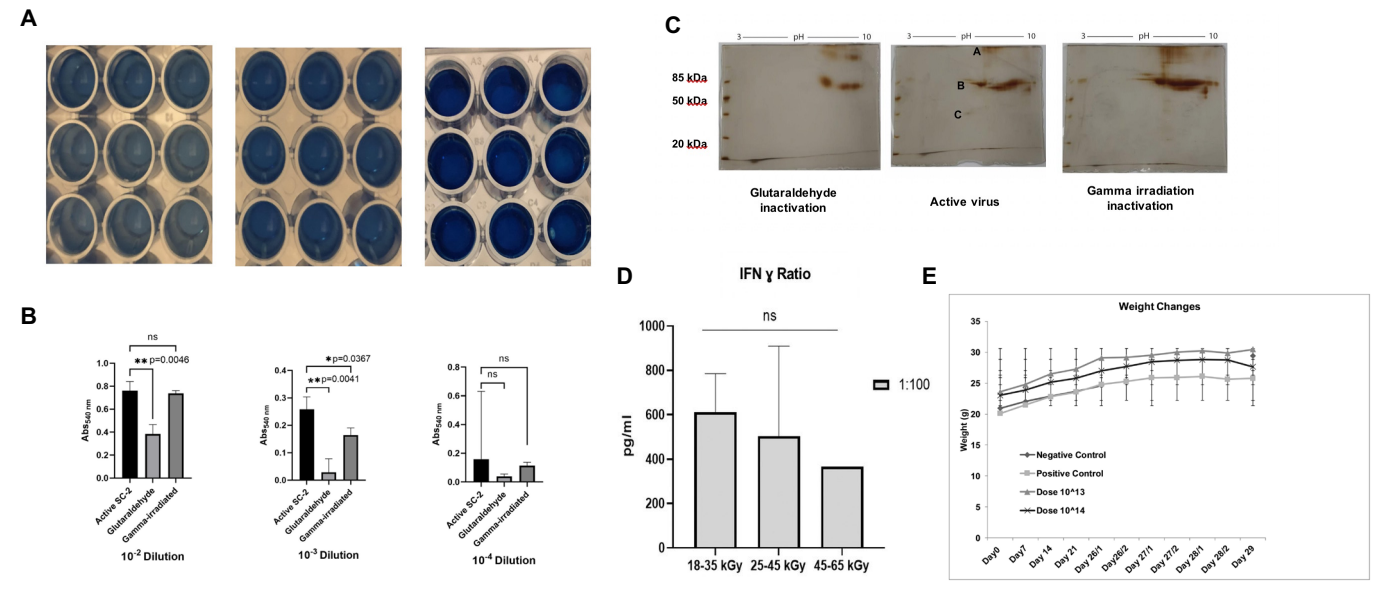


Figure 1. Coomassie Brillant Blue staining (A), bar graph showing viral spike protein expressions results (B), Two-dimensional gel images of samples with active virus, glutaraldehyde and gamma radiation inactivated virus (A: S Protein Domain; B: N Protein Domain; C: M/RBD Protein Domain) (C), bar graph showing IFNy ratio of T cells incubated with OZG-38.61.3 for 24 h (D), Body weight changes during challenge experiments (E). * $p \le .05$, ** $p \le .01$.

3.1.3. The Effect of Gamma Irradiation on the Loss of Viral Proteins

3.1.3.1. Modified Single Immundiffusion Assay Results

After viral spike protein expression, the uptake of SARS-CoV-2 specific spike antibodies by virus particles was followed by the single immundiffusion assay (modified SRID) method. While it was observed that viral spike protein expressions were preserved in an amount similar to the active virus, it was observed that the antigenic expression was significantly decreased in glutaraldehyde-inactivated viral samples. Compared to inactivation with glutaraldehyde, gamma irradiation has been shown to preserve antigenic structure 6 times higher. Gamma-irradiated inactivate vaccine preparation is also a cost-effective approach (Figure 1A, B).

3.1.3.2. 2D Gel Electrophoresis Results

When inactivation by gamma irradiation is compared to inactivation with glutaraldehyde, it is observed that there is a significant loss of protein in inactivation with glutaraldehyde, while proteins are preserved in gamma irradiation. In the analyzes performed after lyophilization, viral proteins could not be clearly evaluated due to the inability to separate from albumin, but a structural change related to protein loss was observed (Figure 1C).

3.1.4. The Effect of Gamma Irradiation on the T cell Stimulation

When different dose of gamma irradiation was evaluated, it was observed that there were no significant changes observed in IFNy ratios of T cell due to gamma irradiation (Figure 1D).

3.2. Challenge Assay Results

3.2.1. Weight changes

Weight monitoring was carried out at regular intervals. No significant difference was found in the parameter (Figure 1E).

3.2.2. Histopathological Examinations Results

3.2.2.1 H&E Staining

Histopathology analysis showed no significant pathological findings in the histological sections of the heart in all groups. However, few hemorrhagic regions were observed in the H&E-stained lung sections of the PC and vaccine groups. Also, it was observed that less hemorrhagic regions were seen in both vaccine doses compared to PC group. These findings suggested that OZG-38.61.3 vaccine protect the lung against the SARS-CoV-2 virus (Figure 2A-D). Histopathological lesions were not observed in the heart sections of control group. Cardiomyocytes with dense eosinophilic cytoplasm were observed in some areas in the Ch1, Ch2. and PC groups. In addition, hypertrophy was observed in some myocardial cells in the PC group. However, no significant difference was observed in the general myocardial architecture in all groups (Figure 2E-H). Kidney tissue morphology was found normal and intact in NC group consisting of the renal tubules and glomeruli. The dilated blood vessels and neutrophil infiltrations were detected in some regions of the PC group kidneys. However, no tubular or glomerular defects were found. Although dilated blood vessels were also seen in vaccinated Ch1 and Ch2 groups, they were much smaller and sparse compared to the NC group and no neutrophils were observed in these groups (Figure 2I-L).

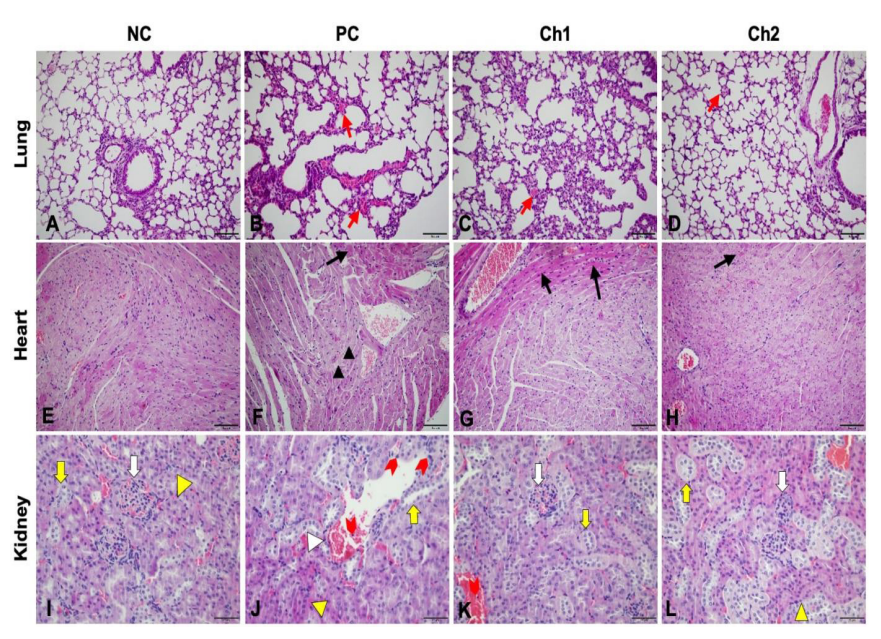


Figure 2. H&E staining of lung, heart and kidney tissues. Red arrows: hemorrhage, Black arrows: cardiomyocytes with dense eosinophilic cytoplasm, Black arrowheads: hypertrophic cardiomyocytes, yellow arrow: distal tubules, Yellow arrowheads: proximal tubules, White arrow: glomeruli, White arrowheads: dilated blood vessel. Scale bar: A-H: 100 µm, I-L: 50 µm.

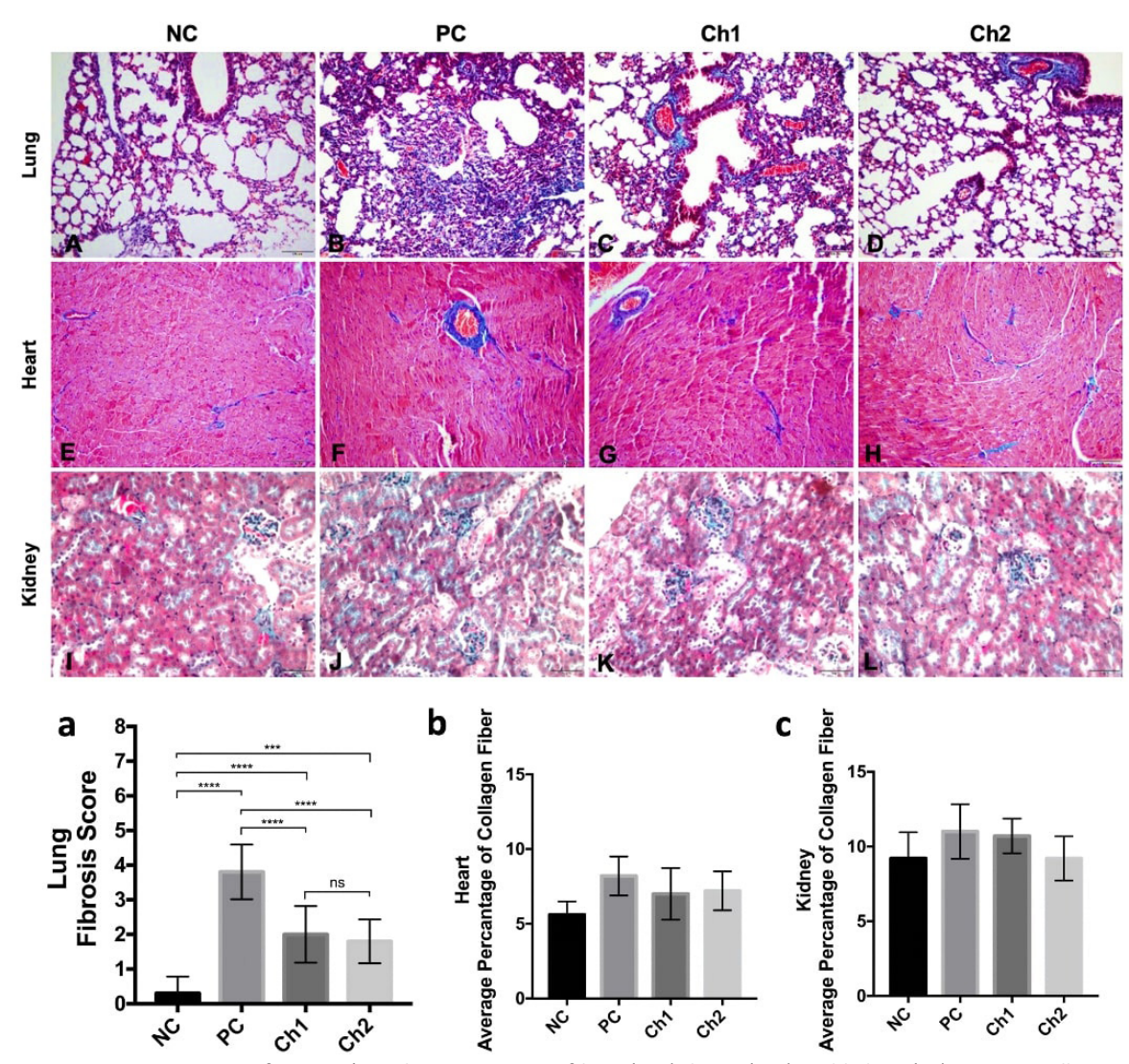


Figure 3. Representative images of Masson's Trichrome Staining of lung (A-D), heart (E-H) and kidney (I-L) tissues in all groups. Statistical analysis graphs of lung fibrosis (a), average percentage of collagen fiber of heart (b) and kidney (c) tissues. ns: p>.05, *** and **** p<.05. Scale bar: A-H: 100 μ m, I-L: 50 μ m

3.2.2.2 Masson's Trichrome Staining

The degree of pulmonary fibrosis was evaluated with ashcroft scoring method as described (13). The highest level of collagen fibers proliferation were observed in the PC group, although vaccine groups had fewer pulmonary fibrosis areas. On the other hand, no abnormal alveolar architecture was noted and a normal distribution of collagen fibers were seen in the NC group. Masson's trichrome staining was demonstrated a moderate thickening of the alveolar septa and increased deposition of collagen in lung tissues in the PC group. Minimal fibrous thickening of the alveolar walls without obvious damage to the lung architecture were observed in the Ch1 and Ch2 groups and the scores of fibrotic lesions were significantly lower in contrast to PC group. Nevertheless, fibrosis scores were similar between vaccine groups. 1x1013 and 1x1014 doses of OZG-38.61.3 were hindered the histopathological changes associated with the SARS-CoV-2 virus (Figure 3A-D, a).

Statistical comparison of collagen fibers area percentages in cardiac and renal tissues of mice revealed that no significant difference were found between the whole groups (Figure 3E-H, b for heart and Figure 3I-L, c for kidney, p>.05).

3.2.2.3. Immunohistochemistry and TUNEL Results

SARS-CoV-2 administration significantly increased the Caspase 3 and iNOS immunoreactivities compared to NC groups in the sections of lung, heart and kidney tissues. However, Caspase 3 immunoreactivity dramatically decreased in the 1x10¹³ and 1x10¹⁴ doses of OZG-38.61.3 vaccinated groups compared to PC groups in a dose dependent manner in all organs. Although, OZG-38.61.3 vaccination led to a statistically significant reduction in iNOS immunoreactivity in lung tissues, iNOS immunostaining intensities were found similar in vaccinated groups in the

heart and kidney tissues compared to PC groups. eNOS immunoreactivity was highest and statistically significant in the PC group of renal tissue however there was no significant difference observed in alveolar and cardiac tissues among all groups (data not shown). In addition to this, vaccine groups had lower eNOS immunoreactivity in the renal tissue in comparison with the PC group. IL-6 immunoreactivity was found highest in the PC groups, and it was statistically significant compared to NC groups in all organs. In the vaccinated groups, IL-6 immunostaining decreased compared to PC groups. Furthermore, OZG-38.61.3 vaccination reduced IL-6 to a similar level to the NC groups. TNF- α immunoreactivity was found similar in all groups of lung and heart tissues (data not shown). Moreover, TNF- α intensity of renal tissue in PC group was significantly higher than NC group. TNF- α intensity reduced with the vaccine and it was significant according to the NC and PC groups. There was no significance between vaccine doses. While IL-10 immunostaining intensity was significantly elevated by SARS-CoV-2 administration in all organs, OZG-38.61.3 vaccinated groups shown lower IL-10 intensity compared to PC groups. TGF-β1 immunoreactivity was found similar between all groups in cardiac and renal tissues. On the other hand, statistically significant increase of TGF-β1 immunoreactivity was observed in the PC group compared the NC group in the lung tissue. In addition,

decreased TGF- $\beta1$ immunoreactivity was seen in the vaccinated groups compared to PC group, and vaccinated groups showed similar TGF- $\beta1$ intensity but still higher than the NC group. The occludin and claudin-1 expressions were similar in lung and heart tissues for all groups (data not shown). In kidney sections, the occludin and claudin-1 immunoreactivity decreased in PC and vaccinated groups, and it was statistically significant according to NC group. High dose OZG-38.61.3 vaccine administration rose the occludin expressions in kidney tissues and it was statistically significant according to PC group although there was no difference between low dose vaccine and PC groups. Claudin-1 intensity increased significantly in both vaccinated groups according to PC group (Figure 4-7, Supplementary Tables 1-3).

The TUNEL assay revealed that extensive amounts of TUNEL positive nuclei were observed in alveolar and vascular areas in lungs, tubular cells in kidneys and endothelial and surrounding cells in cardiac tissues in the SARS-CoV-2 infected groups compared to uninfected controls. In contrast to PC group, apoptotic indexes were found significantly decreased in the OZG-38.61.3 vaccinated groups in a dose dependent manner in all organs. However, there was no significant difference was observed between Ch1 and Ch2 groups in the heart tissue (Figure 9).

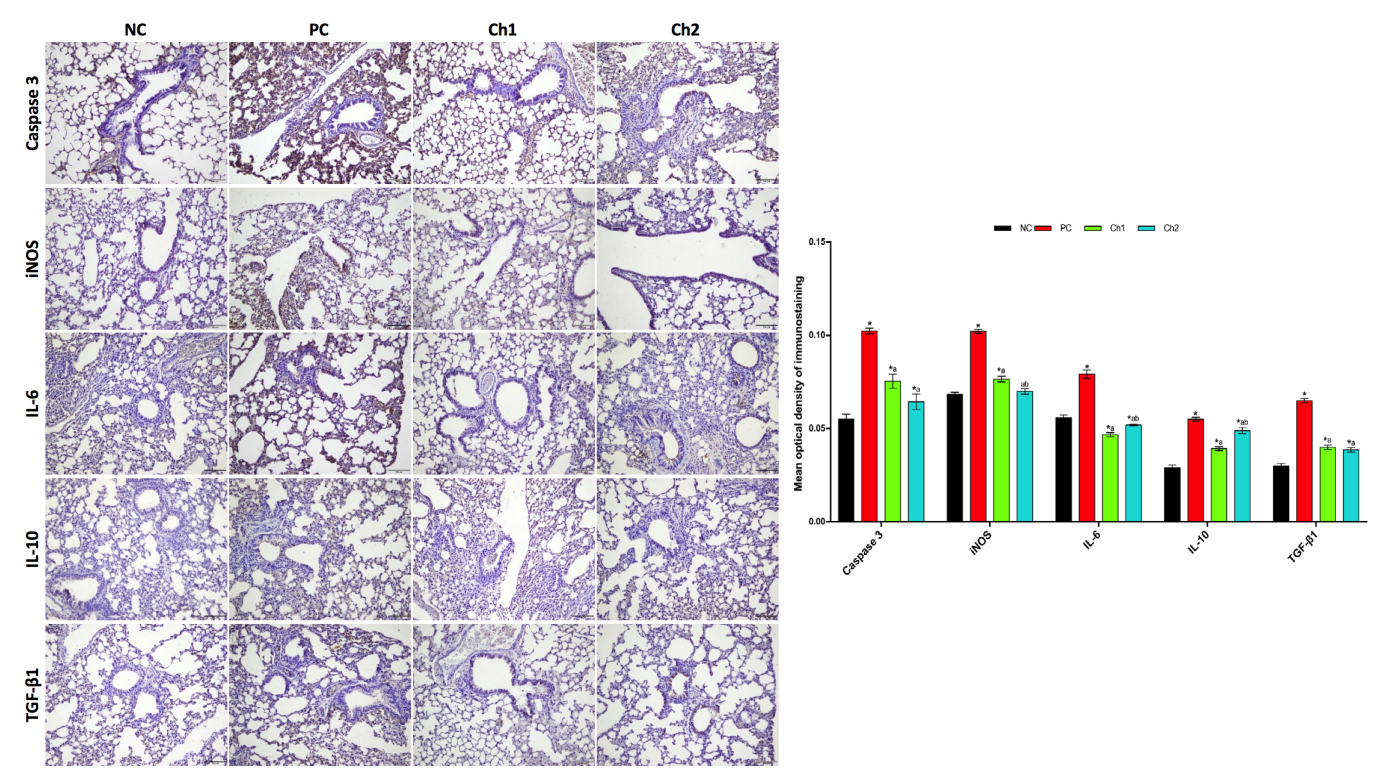


Figure 4. Immunohistochemical analysis of Caspase-3, iNOS, IL-6, IL-10 and TGF- θ in the lung tissues. Scale bar: 100 μ m (100X magnification). Graphs illustrating the optical density of protein expressions in the lung tissues of all groups. *: Comparison with negative control group * p <.05. a: Comparison with positive control group, a = p <.05; b: Comparison with Challenge 1 group, b = p <.05.

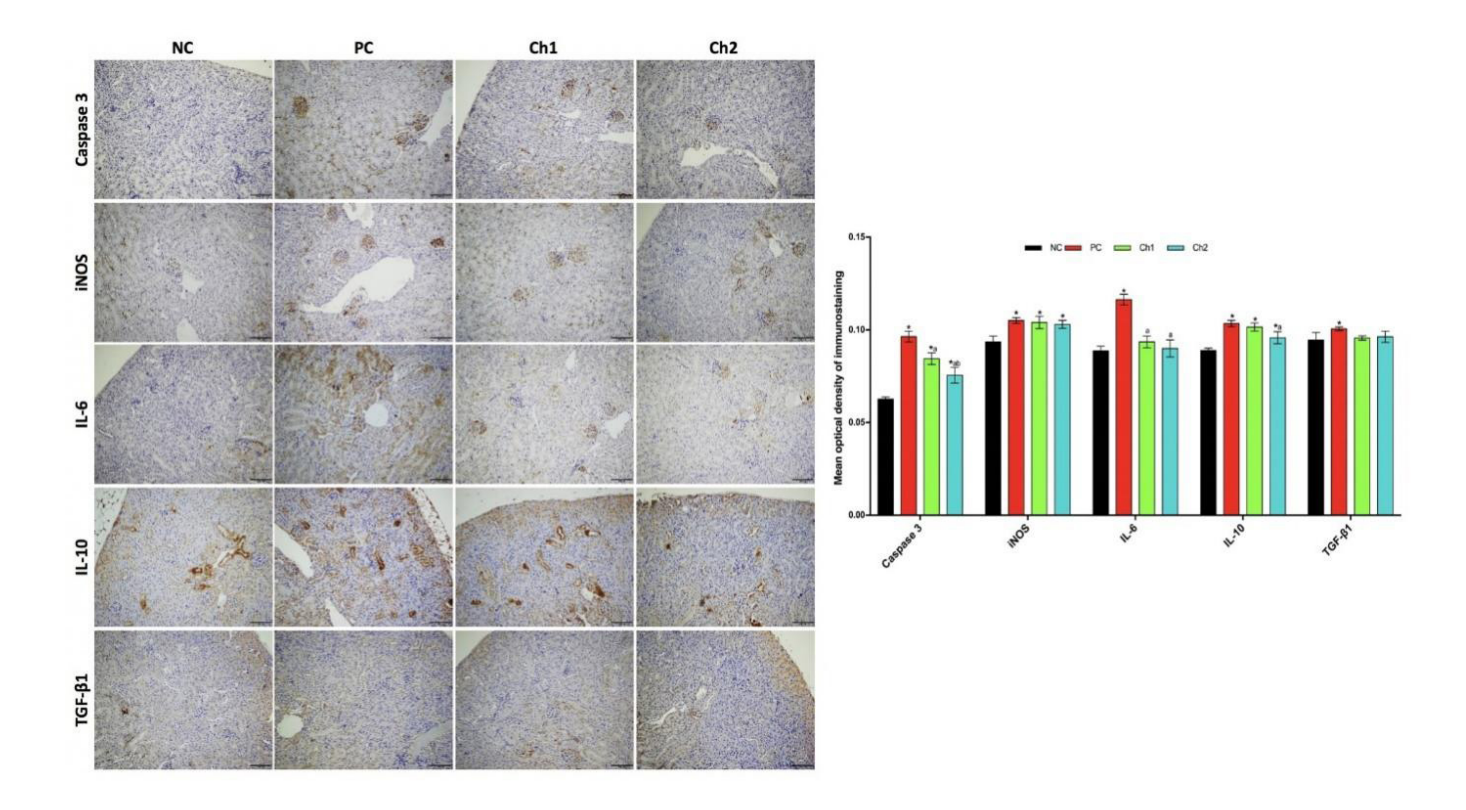


Figure 5. Immunohistochemical analysis of Caspase-3, iNOS, IL-6, IL-10 and TGF-8 in the heart tissues. Scale bar: $100\mu m$ (100X magnification). Graphs illustrating the optical density of protein expressions in the heart tissues of all groups. *: Comparison with negative control group * p < .05. a: Comparison with positive control group, a = p < .05; b: Comparison with Challenge 1 group, b = p < .05.

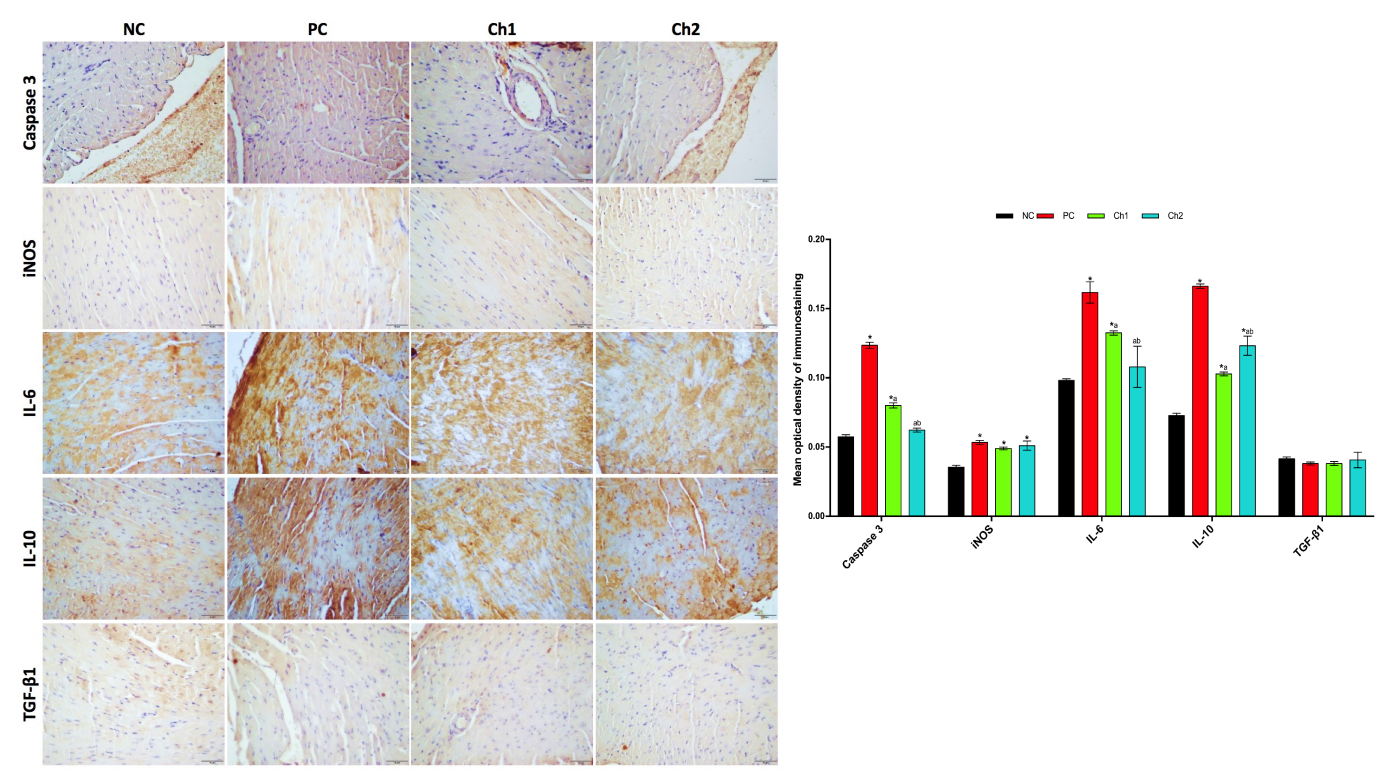


Figure 6. Immunohistochemical analysis of Caspase-3, iNOS, IL-6, IL-10 and TGF- θ in the kidney. Scale bar: 100 μ m (100X magnification). Graphs illustrating the optical density of protein expressions in the kidney tissues of all groups. *: Comparison with negative control group * p <.05. a: Comparison with positive control group, a = p <.05; b: Comparison with Challenge 1 group, b = p <.05.

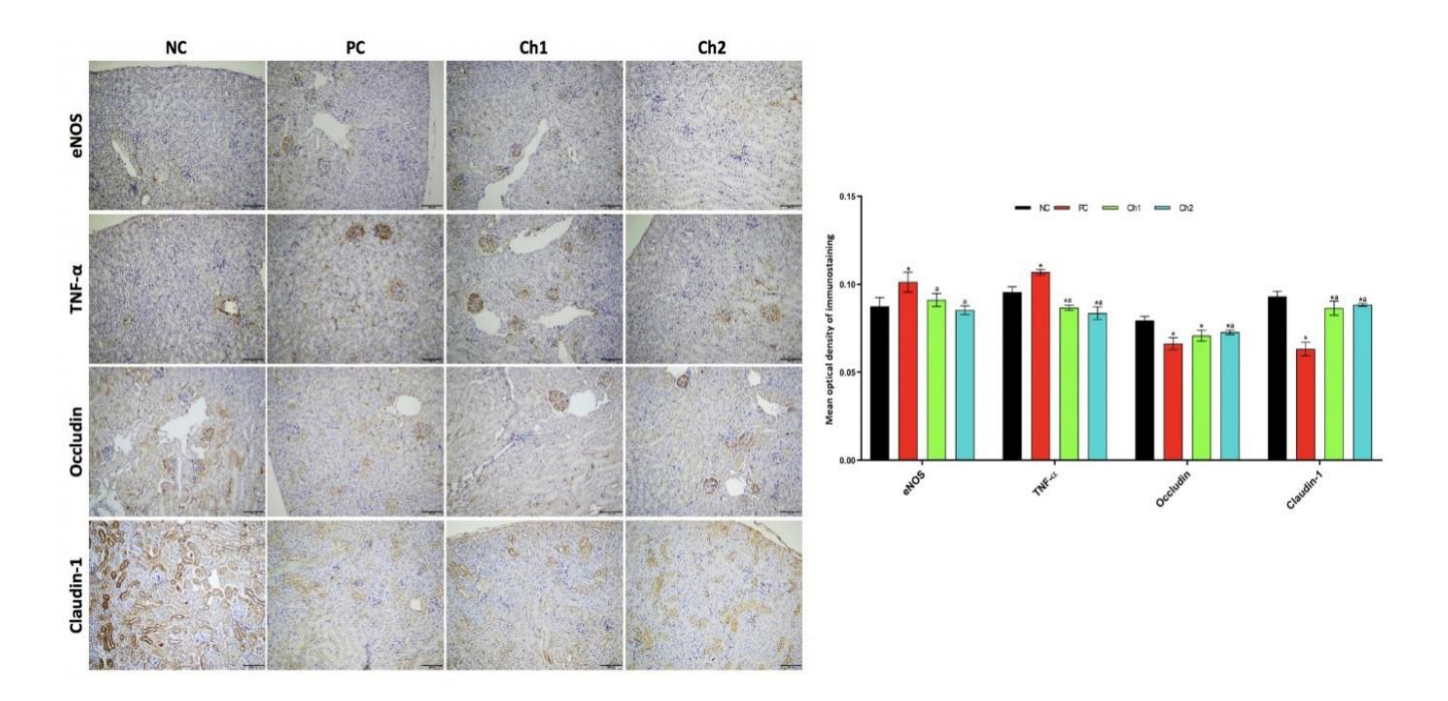


Figure 7. Immunohistochemical analysis of eNOS, TNF- α , Occludin and Claudin-1 in the kidneys. Scale bar: 100 μ m (100X magnification). Graphs illustrating the optical density of protein expressions in the kidneys tissues of all groups. *: Comparison with negative control group * p < .05. a: Comparison with positive control group, a = p < .05; b: Comparison with Challenge 1 group, b = p < .05.

4. DISCUSSION

Several vaccines against SARS-CoV-2 are currently in different stages of pre-clinical or clinical evaluation. In this study, in vivo safety and efficacy analyzes of OZG-38.61.3 lyophilized vaccine candidate, inactivated by gamma-irradiation (25 kGy, determined by kinetics study) were performed. According to comparative analysis carried out by our group, gamma irradiation inactivation was shown to preserve RNA copy number more effectively than chemical inactivation, where 7 times higher viral RNA copy number could be preserved with gamma irradiation. It was also observed that the antigenic expression was significantly decreased in chemically inactivated viral samples, such that gamma irradiation has been shown to preserve antigenic structure 6 times higher. It was seen that there was a significant loss of protein after chemical inactivation, while proteins are preserved in gamma irradiation inactivation. As our results, it has been reported that gamma irradiation method does not cause damage to viral proteins while causing genetic material damage, and therefore it is equivalent to 9 times more antigen gain. These studies also have shown that while chemical inactivation produces only B-cell response, both B-cell and T-cell immunity are induced equally by gamma irradiation (14).

In this viral challenge study, non-lethal doses of SAR-CoV-2 were used for infection. Because, in the past, antibody dependent enhancement (ADE) caused a clinical problem, especially in dengue fever vaccine studies. This ADE effects related to vaccine could not be distinguished in the challenge experiments performed with lethal dose of these studies.

Therefore, this study was designed especially considering the ADE effect in addition to observe the ability of infection control.

To determine the antiviral activity and protective effects of the OZG-38.61.3 against SARS-COV-2 in K18-hACE2 mice, microscopic examination was performed for histopathological changes and also immunohistochemistry was conducted to evaluate the expression of inflammatory cytokines, apoptosis, oxidative stress and cell junction markers in the lung, heart and kidney tissues. Our main findings from the SARS-CoV-2-infected lung tissues of hACE2 mice showed hemorrhagic regions, pulmonary fibrosis and moderate thickening of alveolar septa. The OZG-38.61.3 vaccine prevented these defective effects of the virus but still few hemorrhagic regions and rare septal thickening were detected in the vaccinated lung tissues. The virus-infected heart parenchyma showed cardiomyocytes with dense eosinophilic cytoplasm and hypertrophic cell morphology, which reduced with the vaccine application. Dilated blood vessels and the inflammatory cell infiltration were found in kidney tissues of the infected group. The vaccine ameliorated the renal parenchyma, there were no infiltrating cells. Although a previous study found that COVID-19 increased interstitial fibrosis in the postmortem kidney (15), the collagen fiber deposit was affected by neither the virus infection nor vaccine administration in hearts and kidneys of our animal model. Milross et al (16) reported a lot of lung damages consisting of exudative diffuse alveolar disease

featuring prominent hyaline membranes with mild interstitial infiltration by mononuclear cells, alveolar wall congestion, and cellular debris, platelet-rich thrombus causing expansion of an intra-acinar vessel in post-mortem lung biopsies of COVID-19 patients. Shang et al (17) showed necrosis and abscission in bronchiolar endothelial cells, granulocyte infiltration and thickening alveolar septa in SARS-CoV-2infected lung tissues of hACE2 transgenic mice. Diamond et al (18) detected focal alveolar hemorrhage and immune cell infiltration in SARS-CoV-2-infected Syrian hamsters. Hartman et al (19) reported the severe pericellular interstitial edema around cardiomyocytes and no inflammatory cells in the postmortem heart biopsies of the COVID-19 patients. A similar study was carried out by Pessolani et al (20) and virus-related damage in different organs was examined. They found the necrotic myocytes in myocardium, glomerular capillary microthrombus, tubular dilatation and vacuolisation in kidney tissues of autopsy cases.

Claudin-1 and occludin are tight junction proteins found between epithelial cells. In many studies in the literature, it has been reported that tight junction proteins are disrupted, and their expression decreased after COVID-19 infection (21-23). In particular, it has been reported that the envelope proteins of SARS-CoV-2 disrupt tight junction complexes in cells (21). SARS-CoV-2, by causing tight junction proteins to be damaged, disrupts the barrier function of the respiratory epithelium, thus increasing the spread of the virus rapidly and increasing the severity of the disease (22). In this study, decreased claudin-1 and occludin expressions in kidney tissue were observed in the PC group. There was a significant increase in tight junction protein's expression in the vaccinated groups compared to the PC group. To our knowledge, this is the first study to show the damage of claudin-1 and occludin proteins in kidney tissue after SARS-CoV-2 infection. Herrero et al (24) showed that disruption of the alveleor epithelial barrier as a result of the deterioration of tight junctions causes histopathological findings in the alveoli. Claudin-1 and occludin expressions in kidney tissue were decreased in PC group however, their expressions were increased in the OZG-38.61.3 vaccination groups. These results suggest that the vaccine reduces virus damage.

The specific mechanisms of SARS-CoV-2 infection leading to cell death in different tissues and organs are not fully known. In this study, increased caspase-3 expression and tunnel positive cells were observed in the SARS-CoV-2 positive groups in kidney, lung and heart tissues compared to the control groups. After vaccination with OZG-38.61.3, there was a significant reduction in apoptosis in all tissue types. Increased apoptosis has been reported in postmortem myocardial biopsies of COVID-19 patients. In the study, it is reported that there are very high TUNEL positive cells, especially in endothelial cells (19). Tavazzi et al (25) reported that oxidative stress, hypoxia, intrarenal inflammatory response and renal cell apoptosis are the main mechanisms of sepsis-associated kidney injury. Li et al (26) reported that by providing caspase-8 activation in lung epithelial cells of transgenic HFH4-hACE2 mice infected with SARS-CoV-2, it

triggered the inflammatory cytokine storm with intrinsic and extrinsic apoptosis pathways. Initially, virus-induced apoptosis is thought to be beneficial for the host cell in restricting viral replication. However, hyperactivation of these pathways causes serious tissue and organ damage as seen in our study and in the literature.

After SARS-CoV-2 enters the body and replicates rapidly, a rapid cytokine release triggers inflammation. Thus, it has been reported that the main cause of tissue damage is increased inflammation (27,28). Lindner et al (29) reported that severe damage to the myocardium was associated with high TNF- α , IFN, IL-1B, IL-6 levels in the autopsy performed on patients who died as a result of SARS-CoV-2 infection. It is reported that one of the most important triggers of these inflammatory cytokines is NF-κB (27). NF-κB inhibition has been reported to decrease proinflammatory cytokine expressions and increase survival rate in SARS-CoV infected mice (30). In our study, increased TNF- α expression was observed in the PC group. However, a significant decrease in TNF- α levels was observed after the administered OZG-38.61.3 vaccine. This shows that the vaccine candidate is highly effective in eliminating SARS-CoV-2 virus-induced inflammation.

Several studies have suggested that SARS-CoV-2 has an important function in the pathogenesis of the disease by increasing the excessive production of ROS in the cells (31). In our study, iNOS and eNOS, which are oxidative stress markers, showed a significant increase in the PC group compared to the control group. However, although there was a certain decrease in the vaccine group, it was not statistically significant. The role of oxidative stress triggered by COVID-19 infection in the pathogenesis of the disease is still not fully known. On the other hand, oxidative stress induces overactivation of the immune response of infected cells affected by SARS-CoV-2 replication (32). In particular, proinflammatory cytokines IL-1β, IL-6, TNF-α, IL-8 secreted from monocytes and macrophages rapidly trigger an increase in oxidative stress in other cells (33). As shown in our study, it is thought that the increased oxidative stress in the lung, kidney and heart tissues may be caused by the increase in IL-6, TNF- α , IL-10. It has been reported that in addition to immune cells, mast cell activation is also increased after viral infections, and TNF- α released from mast cells plays a role in increasing local inflammation (18).

The Arg-Gly-Asp (RGD)-binding sites required for SARS-CoV-2 to bind to the host cell surface trigger TGF- β activation in the cells and this provides a severe course of the disease (34). TGF- β provides the organization of the extracellular matrix by controlling the fibroblast-myofibroblast transformation. There is evidence that TGF- β is closely related to the fibrogenic process (35). In our study, increased TGF- β expression and increased fibrosis in the lung tissues in the PC group support this situation. At the same time, the increase in TGF- β provides a rapid increase in proinflammatory cytokines, as in our study. The decrease in TGF- β expressions of the vaccine candidate in our study caused a decrease in morphologically fibrotic areas in the lung tissue. Several animal models have

shown that the TGF- β /Smad signaling pathway plays an important role in renal fibrosis (36). In our study, increased TGF- β expression was observed in the PC group kidney tissue compared to the NC group. Although a slight decrease was observed in the vaccinated groups, it was not found to be statistically significant.

5. CONCLUSION

In this study, it was shown that SARS-CoV-2 infection can cause multi-organ involvement other than the lung, and it was determined that the OZG-38.61 vaccine candidate could clearly control the organ dysfunction caused by SARS-CoV-2 infection. And it was observed that there was an infection control with no ADE effect.

Acknowledgements: Selen Abanuz is supported by the TUBITAK-BIDEB 2244-University-Industry Ph.D. program, project number 118C082. Sevda Demir is funded by TUBITAK 2247-C Trainee Researcher Scholarship Program (STAR).

Funding: The author(s) received no financial support for the research. All funding in the work was supported by Celltek Health and Consulting Services Limited Company.

Conflicts of interest: The authors declare that they have no conflict of interest.

Ethics Committee Approval: All animal experiments were approved by the Experimental Animal Committee of Acıbadem Mehmet Ali Aydınlar University (ACUHADYEK 2020/36) and Manisa Celal Bayar University (2020/18). The animal research in our study adheres to the ARRIVE guidelines (https://arriveguidelines.org/arriveguidelines).

Peer-review: Externally peer-reviewed.

Author Contributions:

Research idea: MO, HO, DDK, EO

Design of the study: MO, HO, DDK, CT, DT, EO

Acquisition of data for the study: DDK, CT, BY, DC, SA, MK, GA, MO, HO, BSH

Analysis of data for the study: DDK, CT, BY, DC, SA, GT, SD, DT, MK, GA, MO, HO, BSH

Interpretation of data for the study: MO, HO, DDK, CT, SA, DT, EO Drafting the manuscript: MO, HO, DDK

Revising it critically for important intellectual content: EO Final approval of the version to be published: MO, DDK, HO, RDT, GSK, BY, DÇ, SA, CT, SO, GT, MK, GA, BSH, SD, ST, FS, MIT, EO

Data Availability: No datasets were generated or analysed during the current study.

REFERENCES

- [1] Soy M, Keser G, Atagündüz P, Tabak F, Atagündüz I, Kayhan S. Cytokine storm in COVID-19: pathogenesis and overview of anti-inflammatory agents used in treatment. Clin Rheumatol. 2020;39(7):2085-2094. https://doi.org/10.1007/s10067.020.05190-5.
- [2] Frisoni P, Neri M, D'Errico S, Alfieri L, Bonuccelli D, Cingolani M, Di Paolo M, Gaudio RM, Lestani M, Marti M, Martelloni M, Moreschi C, Santurro A, Scopetti M, Turriziani O, Zanon M, Scendoni R, Frati P, Fineschi V. Cytokine storm and histopathological findings in 60 cases of COVID-19-related death: From viral load research to immunohistochemical quantification of major players IL-1β, IL-6, IL-15 and TNF-α.

- Forensic Sci Med Pathol. 2021;1-15. https://doi.org/10.1007/s12024.021.00414-9.
- [3] Ke Z, Oton J, Qu K, Cortese M, Zila V, McKeane L, Nakane T, Zivanov J, Neufeldt CJ, Cerikan B, Lu JM, Peukes J, Xiong X, Kräusslich HG, Scheres SHW, Bartenschlager R, Briggs JAG. Structures and distributions of SARS-CoV-2 spike proteins on intact virions. Nature 2020;588(7838):498-502. https://doi.org/10.1038/s41586.020.2665-2.
- [4] Lean FZX, Lamers MM, Smith SP, Shipley R, Schipper D, Temperton N, Haagmans BL, Banyard AC, Bewley KR, Carroll MW, Brookes SM, Brown I, Nuñez A. Development of immunohistochemistry and in situ hybridization for the detection of SARS-CoV and SARS-CoV-2 in formalin-fixed paraffin-embedded specimens. Sci Rep. 2020;10(1):1-9. https://doi.org/10.1038/s41598.020.78949-0.
- [5] Sia, S. F., Yan, L. M., Chin AWH, Fung K., Choy K. T., Wong AYL, Kaewpreedee P., Perera RAPM, Poon LLM, Nicholls JM, Peiris M., Yen H.-L. Pathogenesis and transmission of SARS-CoV-2 in golden hamsters. Nature 2020;583(7818):834-838. https:// doi.org/10.1038/s41586.020.2342-5.
- [6] Turan RD, Tastan C, Dilek Kancagi D, Yurtsever B, Sir Karakus G, Ozer S, Abanuz S, Cakirsoy D, Tumentemur G, Demir S, Seyis U, Kuzay R, Elek M, Kocaoglu ME, Ertop G, Arbak S, Acikel Elmas M, Hemsinlioglu C, Hatirnaz Ng O, Akyoney S, Sahin I, Kayhan CK, Tokat F, Akpinar G, Kasap M, Kocagoz AS, Ozbek U, Telci D, Sahin F, Yalcin K, Ratip S, Ince U, Ovali E. Gammairradiated SARS-CoV-2 vaccine candidate, OZG-38.61.3, confers protection from SARS-CoV-2 challenge in human ACEII-transgenic mice. Sci Rep. 2021;11(1):15799. https://doi.org/10.1038/s41598.021.95086-4.
- [7] Sir Karakus G, Tastan C, Dilek Kancagi D, Yurtsever B, Tumentemur G, Demir S, Turan RD, Abanuz S, Cakirsoy D, Seyis U, Ozer S, Elibol O, Elek M, Ertop G, Arbak S, Acikel Elmas M, Hemsinlioglu C, Kocagoz AS, Hatirnaz Ng O, Akyoney S, Sahin I, Ozbek U, Telci D, Sahin F, Yalcin K, Ratip S, Ovali E. Preclinical efficacy and safety analysis of gamma-irradiated inactivated SARS-CoV-2 vaccine candidates. Sci Rep. 2021;11(1):5804. https://doi.org/10.1038/s41598.021.83930-6.
- [8] Williams, M.S. 1993. Single-radial-immunodiffusion as an in vitro potency assay for human inactivated viral vaccines. Vet Microbiol. 1993;37(3-4):253-62. https://doi. org/10.1016/0378-1135(93)90027-5.
- [9] Taştan C, Yurtsever B, Sir Karakuş G, Dilek Kançaği D, Demir S, Abanuz S, Seyis U, Yildirim M, Kuzay R, Elibol Ö, Arbak S, Açikel Elmas M, Birdoğan S, Sezerman OU, Kocagöz AS, YalÇin K, Ovali E. SARS-CoV-2 isolation and propagation from Turkish COVID-19 patients. Turk J Biol. 2020;44(3):192-202. https://doi.org/10.3906/biy-2004-113.
- [10] Eren SA, Tastan C, Karadeniz KB, Turan RD, Cakirsoy D, Kancagi DD, Yilmaz SU, Oztatlici M, Oztatlici H, Ozer S, Tumentemur G, Baykal AT, Ovali E. Lentiviral micro-dystrophin gene treatment into late-stage mdx mice for Duchene Muscular Dystrophy disease. Curr. Gene Ther. 2023;23:304–315.
- [11] Birinci, H., Vatansever, H. S., Yüncü, M. Effect of kisspeptin-54 on ovarian levels of pigment epithelium-derived factor (PEDF) and vascular endothelial growth factor (VEGF) in an experimental model of ovarian hyperstimulation syndrome (OHSS). Reprod Fertil Dev. 2021;33(16):799-809. https://doi.org/10.1071/RD21140.
- [12] Özbilgin, M. K., Demirören, S., Üçöz, M., Oztatlici, M. Cyclophosphamide suppresses spermatogenesis in the testis of mice through downregulation of miR-34b and miR-34c.

- Andrologia. 2012;53(7):e14071. https://doi.org/10.1111/and.14071.
- [13] Liu, M. W., Su, M. X., Tang, D. Y., Hao, L., Xun, X. H., Huang, Y. Q. Ligustrazin increases lung cell autophagy and ameliorates paraquat-induced pulmonary fibrosis by inhibiting PI3K/Akt/mTOR and hedgehog signalling via increasing miR-193a expression. BMC Pulm Med. 2019;19(1):35. https://doi.org/10.1186/s12890.019.0799-5.
- [14] Abolaban, F. A., Djouider, F.M. Gamma irradiation-mediated inactivation of enveloped viruses with conservation of genome integrity: Potential application for SARS-CoV-2 inactivated vaccine development. Open Life Sci. 2021;16(1), 558-570. https://doi.org/10.1515/biol-2021-0051.
- [15] Jansen J, Reimer KC, Nagai JS, Varghese FS, Overheul GJ, de Beer M, Roverts R, Daviran D, Fermin LAS, Willemsen B, Beukenboom M, Djudjaj S, von Stillfried S, van Eijk LE, Mastik M, Bulthuis M, Dunnen WD, van Goor H, Hillebrands JL, Triana SH, Alexandrov T, Timm MC, van den Berge BT, van den Broek M, Nlandu Q, Heijnert J, Bindels EMJ, Hoogenboezem RM, Mooren F, Kuppe C, Miesen P, Grünberg K, Ijzermans T, Steenbergen EJ, Czogalla J, Schreuder MF, Sommerdijk N, Akiva A, Boor P, Puelles VG, Floege J, Huber TB. SARS-CoV-2 infects the human kidney and drives fibrosis in kidney organoids. Cell Stem Cell 2021;29(2):217-231. https://doi.org/10.1016/j. stem.2021.12.010
- [16] Milross, L., Majo, J., Cooper, N., Kaye, P. M., Bayraktar, O., Filby, A., Fisher, A. J. Post-mortem lung tissue: the fossil record of the pathophysiology and immunopathology of severe COVID-19. Lancet Respir Med. 2022;10(1):95-106. https://doi. org/10.1016/s2213-2600(21)00408-2.
- [17] Shang C, Zhuang X, Zhang H, Li Y, Zhu Y, Lu J, Ge C, Cong J, Li T, Li N, Tian M, Jin N, Li X. Inhibition of Autophagy Suppresses SARS-CoV-2 Replication and Ameliorates Pneumonia in hACE2 Transgenic Mice and Xenografted Human Lung Tissues. J Virol. 2021;95(24):e0153721. https://doi.org/10.1128/JVI.01537-21.
- [18] Halfmann PJ, Iida S, Iwatsuki-Horimoto K, Maemura T, Kiso M, Scheaffer SM, Darling TL, Joshi A, Loeber S, Singh G, Foster SL, Ying B, Case JB, Chong Z, Whitener B, Moliva J, Floyd K, Ujie M, Nakajima N, Ito M, Wright R, Uraki R, Warang P, Gagne M, Li R, Sakai-Tagawa Y, Liu Y, Larson D, Osorio JE, Hernandez-Ortiz JP, Henry AR, Ciuoderis K, Florek KR, Patel M, Odle A, Wong LR, Bateman AC, Wang Z, Edara VV, Chong Z, Franks J, Jeevan T, Fabrizio T, DeBeauchamp J, Kercher L, Seiler P, Gonzalez-Reiche AS, Sordillo EM, Chang LA, van Bakel H, Simon V; Consortium Mount Sinai Pathogen Surveillance (PSP) study group; Douek DC, Sullivan NJ, Thackray LB, Ueki H, Yamayoshi S, Imai M, Perlman S, Webby RJ, Seder RA, Suthar MS, García-Sastre A, Schotsaert M, Suzuki T, Boon ACM, Diamond MS, Kawaoka Y. SARS-CoV-2 Omicron virus causes attenuated disease in mice and hamsters. Nature. 2022 Mar;603(7902):687-692. https:// doi.org/10.1038/s41586.022.04441-6.
- [19] Hartmann, C., Miggiolaro, A. F. R. D. S., Motta, J. D. S. J., Baena Carstens, L., Busatta Vaz De Paula, C., Fagundes Grobe, S., de Souza Nunes, L. H., Marques, G. L., Libby, P., Moura, L. Z., de Noronha, L., Pellegrino Baena, C. The Pathogenesis of COVID-19 myocardial injury: An immunohistochemical study of postmortem biopsies. Front Immunol. 2021;12:748417. https://doi.org/10.3389/fimmu.2021.748417.
- [20] Pessolani, T. G., de Legaria, M. M. F., Apellániz, M. E., Moreno, S. S., Cortés, M. D. M. L., Sánchez, S. G. Multi-organ pathological findings associated with COVID-19 in postmortem needle

- core biopsies in four patients and a review of the current literature. Rev Esp Patol. 2021;54(4), 275-280. https://doi.org/10.1016/j.patol.2020.09.003
- [21] De Maio, F., Cascio, E. L., Babini, G., Sali, M., Della Longa, S., Tilocca, B., Roncada, P., Arcovito, A., Sanguinetti, M., Scambia, G., Urbani, A. Improved binding of SARS-CoV-2 Envelope protein to tight junction-associated PALS1 could play a key role in COVID-19 pathogenesis. Microbes Infect. 2020;22(10):592-597. https://doi.org/10.1016/j.micinf.2020.08.006.
- [22] Shepley-McTaggart A, Sagum CA, Oliva I, Rybakovsky E, DiGuilio K, Liang J, Bedford MT, Cassel J, Sudol M, Mullin JM, Harty RN. SARS-CoV-2 Envelope (E) protein interacts with PDZ-domain-2 of host tight junction protein ZO1. PLoS One 2021;16(6):e0251955. https://doi.org/10.1371/journal. pone.0251955.
- [23] Stewart CA, Gay CM, Ramkumar K, Cargill KR, Cardnell RJ, Nilsson MB, Heeke S, Park EM, Kundu ST, Diao L, Wang Q, Shen L, Xi Y, Zhang B, Della Corte CM, Fan Y, Kundu K, Gao B, Avila K, Pickering CR, Johnson FM, Zhang J, Kadara H, Minna JD, Gibbons DL, Wang J, Heymach JV, Byers LA. Lung cancer models reveal SARS-CoV-2-induced EMT contributes to COVID-19 pathophysiology. bioRxiv. 2021;2020.05.28.122291. https://doi.org/10.1101/2020.05.28.122291. Update in: J Thorac Oncol. 2021 Nov;16(11):1821-1839.
- [24] Herrero, R., Sanchez, G., Lorente, J. A. New insights into the mechanisms of pulmonary edema in acute lung injury. Ann Transl Med. 2018;6(2):32. https://doi.org/10.21037/atm.2017.12.18.
- [25] Tavazzi G, Pellegrini C, Maurelli M, Belliato M, Sciutti F, Bottazzi A, Sepe PA, Resasco T, Camporotondo R, Bruno R, Baldanti F, Paolucci S, Pelenghi S, Iotti GA, Mojoli F, Arbustini E. Myocardial localization of coronavirus in COVID-19 cardiogenic shock. Eur J Heart Fail. 2020;22(5):911-915. https://doi.org/10.1002/ejhf.1828.
- [26] Li S, Zhang Y, Guan Z, Li H, Ye M, Chen X, Shen J, Zhou Y, Shi ZL, Zhou P, Peng K. SARS-CoV-2 triggers inflammatory responses and cell death through caspase-8 activation. Signal Transduct Target Ther. 2020;5(1):235. https://doi.org/10.1038/ s41392.020.00334-0.
- [27] Shi Y, Wang Y, Shao C, Huang J, Gan J, Huang X, Bucci E, Piacentini M, Ippolito G, Melino, G. COVID-19 infection: the perspectives on immune responses. Cell Death Differ. 2020;27(5):1451-1454. https://doi.org/10.1038/s41418.020.0530-3.
- [28] Ho HT, Peischard S, Strutz-Seebohm N, Klingel K, Seebohm G. Myocardial damage by sars-cov-2: Emerging mechanisms and therapies. Viruses. 2021;13(9):1880. https://doi.org/10.3390/ v13091880
- [29] Lindner D, Fitzek A, Bräuninger H. Association of cardiac infection with sars-cov-2 in confirmed covid-19 autopsy cases. JAMA Cardiol. 2020;5(11):1281-1285. https://doi. org/10.1001/jamacardio.2020.3551.
- [30] DeDiego, M. L., Nieto-Torres, J. L., Regla-Nava, J. A., Jimenez-Guardeño, J. M., Fernandez-Delgado, R., Fett, C., Castano-Rodriguez, C., Perlman, S., Enjuanes, L. Inhibition of NF-κB-mediated inflammation in severe acute respiratory syndrome coronavirus-infected mice increases survival. J Virol. 2014;88(2):913-24. https://doi.org/10.1128/JVI.02576-13.
- [31] Delgado-Roche, L., Mesta, F. Oxidative Stress as Key Player in Severe Acute Respiratory Syndrome Coronavirus (SARS-CoV) Infection. Arch Med Res. 2020;51(5):384-387. https://doi.org/10.1016/j.arcmed.2020.04.019.

- [32] Chernyak, B. V., Popova, E. N., Prikhodko, A. S., Grebenchikov, O. A., Zinovkina, L. A., Zinovkin, R. A. COVID-19 and Oxidative Stress. Biochemistry (Mosc). 2020;85(12):1543-1553. https:// doi.org/10.1134/S000.629.7920120068.
- [33] Mehta P, McAuley DF, Brown M, Sanchez E, Tattersall RS, Manson JJ, HLH Across Speciality Collaboration, UK. COVID-19: Consider cytokine storm syndromes and immunosuppression. Lancet 2020;395(10229):1033-1034. https://doi.org/10.1016/ S0140-6736(20)30628-0.
- [34] Carvacho I, Piesche M. RGD-binding integrins and TGF- β in SARS-CoV-2 infections novel targets to treat COVID-19

- patients? Clin Transl Immunology. 2021;10(3):e1240. https://doi.org/10.1002/cti2.1240.
- [35] Vaz de Paula CB, Nagashima S, Liberalesso V, Collete M, da Silva FPG, Oricil AGG, Barbosa GS, da Silva GVC, Wiedmer DB, da Silva Dezidério F, Noronha L. COVID-19: Immunohistochemical analysis of tgf-β signaling pathways in pulmonary fibrosis. Int J Mol Sci. 2021;23(1):168. https://doi.org/10.3390/ijms23010168.
- [36] Xu L, Tan B, Huang D, Yuan M, Li T, Wu M, Ye C. Remdesivir inhibits tubulointerstitial fibrosis in obstructed kidneys. Front Pharmacol. 2021;12:626510. https://doi.org/10.3389/fphar.2021.626510.

Supplementary Table 1. Lung tissue optical density of immunostaining (mean ± standard deviation)

Lung	Negative Control	Positive Control	Challenge 1	Challenge 2
Caspase 3	0.055±0.003	0.102±0.002*	0.080±0.002*a	0.062±0.001*a
iNOS	0.068±0.001	0.102±0.001*	0.077±0.002*a	0.070±0.001 ^{ab}
IL-6	0.056±0.002	0.079±0.002*	0.047±0.001*a	0.052±0.000*ab
IL-10	0.029±0.001	0.057±0.001*	0.039±0.001*a	0.046±0.002*ab
TGF-β1	0.030±0.001	0.065±0.001*	0.040±0.001*a	0.039±0.001*a

^{*:} Comparison with negative control group * p <.05. a: Comparison with positive control group, a = p <.05; b: Comparison with Challenge 1 group, b = p <.05

Supplementary Table 2. Heart tissue optical density of immunostaining (mean ± standard deviation)

Heart	Negative Control	Positive Control	Challenge 1	Challenge 2
Caspase 3	0.057±0.002	0.124±0.002*	0.078±0.002*a	0.062±0.001 ^{ab}
iNOS	0.036±0.001	0.053±0.002*	0.049±0.001*	0.051±0.003*
IL-6	0.098±0.001	0.162±0.008*	0.132±0.002*a	0.108±0.015 ab
IL-10	0.073±0.002	0.166±0.002*	0.108±0.001*a	0.123±0.007*ab
TGF-β1	0.043±0.001	0.038±0.001	0.038±0.001	0.041±0.006

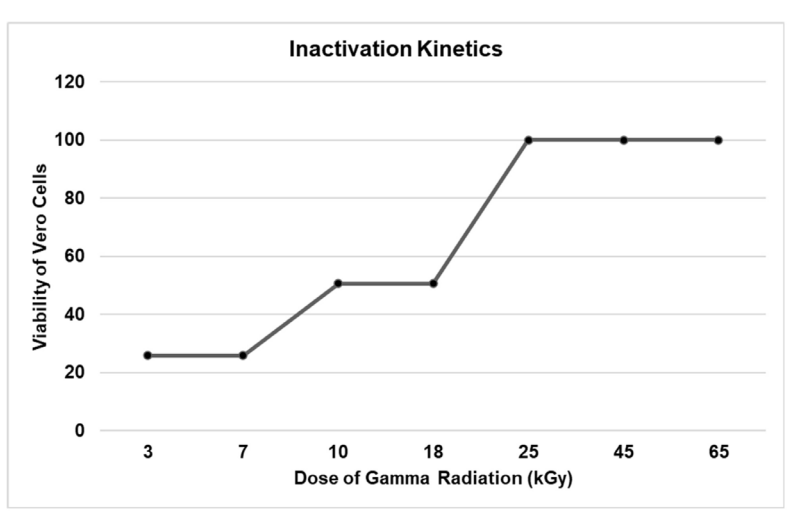
^{*:} Comparison with negative control group * p < .05. a: Comparison with positive control group, a = p < .05; b: Comparison with Challenge 1 group, b = p < .05

Supplementary Table 3. Kidney tissue optical density of immunostaining (mean ± standard deviation)

Kidney	Negative Control	Positive Control	Challenge 1	Challenge 2
Caspase 3	0.063 ± 0.001	0.096 ± 0.002*	0.084 ± 0.003*a	0.076 ± 0.004*ab
iNOS	0.091 ± 0.003	0.105 ± 0.002*	0.104 ± 0.003*	0.103 ± 0.002*
IL-6	0.089 ± 0.002	0.116 ± 0.011*	0.094 ± 0.003°	0.090 ± 0.004 ^a
IL-10	0.089 ± 0.001	0.103 ± 0.001*	0.102 ± 0.002*	0.096 ± 0.003*a
TGF-β1	0.094 ± 0.003	0.101 ± 0.002*	0.096 ± 0.001	0.096 ± 0.002
eNOS	0.087 ± 0.004	0.101 ± 0.002*	0.091 ± 0.003°	0.085 ± 0.002°
TNF-α	0.095 ± 0.003	0.107 ± 0.010*	0.087 ± 0.001*a	0.084 ± 0.003*a
Occludin	0.079 ± 0.002	0.066 ± 0.004*	0.071 ± 0.003*	0.073 ± 0.001*a
Claudin-1	0.093 ± 0.002	0.063 ± 0.011*	0.086 ± 0.003*a	0.088 ± 0.001*a

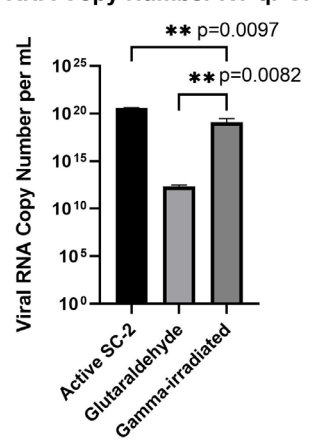
^{*:} Comparison with negative control group * p <.05. a: Comparison with positive control group, a = p <.05; b: Comparison with Challenge 1 group, b = p <.05





В

Viral RNA Copy Number RT-qPCR Results



Supplementary Figure 1. Inactivation kinetics of gamma irradiation (A), bar graph showing quantitative RT-PCR results of SARS-CoV-2 viral RNA copy number in log scale (B). ** p < .01.